Available online at www.sciencedirect.com
ScienceDirect
International Journal of Heat and Mass Transfer 50 (2007) 1485–1499
International Journal of HEAT and MASS TRANSFER
www.elsevier.com/locate/ijhmt

Spatio-temporal stability analysis of mixed convection flows in porous media heated from below: Comparison with experiments

A. Delache [a], M.N. Ouarzazi [a,*], M. Combarnous [b]

[a] Laboratoire de Mécanique de Lille, UMR CNRS 8107, USTL, bd. Paul Langevin, 59655 Villeneuve d'Ascq Cedex, France
[b] Laboratoire TREFLE (TRansferts Ecoulements FLuides Energétique) UMR CNRS 8508, ENSAM, Esplanade des Arts et Métiers, F-33405 Talence Cedex, France

Received 30 May 2006; received in revised form 21 July 2006
Available online 28 November 2006

Abstract

We consider a stability analysis of a fluid in a porous layer heated from below including the effects of a superposed through-flow, porous inertia and the lateral confinement of the medium with respect to extended and localized perturbations. It is found that extended perturbations promote the appearance of down-stream moving transverse modes (T modes) provided that the Péclet number Pe remains below a critical value Pe^*. We showed that the T modes are replaced by stationary longitudinal rolls (L rolls) if $Pe > Pe^*$. On the other hand when localized perturbations are considered, a spatial stability analysis is performed to determine regions of convective and absolute instability for T modes as well as for L rolls in the filtration Rayleigh–Péclet plane. We found that while the lateral aspect ratio has a strong influence on the convective/absolute nature of secondary flows, the main effect of porous inertia is to delay the transition to the absolute instability. Quantitative comparisons between our finding and experimental results published by one of us (M.C.) are presented. As far as the solid thermal conductivity is similar to that of the fluid, it is found that the experimentally observed transition between the T modes and L rolls occurs at the border between convective and absolute instability. Moreover it has also been found that the measured and the theoretically predicted wavelengths of T modes as well as their period of oscillation are in good agreement for various combinations of Ra and Pe numbers. The agreement between theory and experiment becomes less satisfactory when the matrix is much more conductive than the fluid. Therefore the assumption of local thermal equilibrium between solid and fluid becomes debatable.

Keywords: Mixed convection; Porous media; Absolute instability

1. Introduction

The stability of convection in a fluid medium heated from below and cooled from above with a super-imposed through-flow have been extensively investigated in the past two decades. In this so called Poiseuille–Rayleigh–Bénard (PRB) problem various vortex flow structures such as steady longitudinal rolls (L rolls) with their rotation axes parallel to the through-flow direction, down-stream moving transverse rolls (T rolls) with their rotation axes perpendicular to the through-flow direction, mixed L rolls and T rolls, and irregular cells have been reported in the literature. To delineate the vortex patterns in the medium, detailed experimental flow visualizations and Laser Doppler Anemometry measurements [1–3] were conducted covering wide ranges of the governing parameters. On the other hand among the most comprehensive and recent linear stability analysis of the PRB problem, let us cite the study of Nicolas et al. [4] and the work of Carrière and Monkewitz [5]. We urge the reader interested in learning more about the PRB problem to consult an exhaustive bibliographical review on this subject which has been presented recently by Nicolas [6]. This excellent review covers the period 1920–2001 and counts 154 references.

* Corresponding author. Tel.: +33 320434261; fax: +33 320337088.
E-mail address: najib.ouarzazi@univ-lille1.fr (M.N. Ouarzazi).

0017-9310/$ - see front matter © 2006 Elsevier Ltd. All rights reserved.
doi:10.1016/j.ijheatmasstransfer.2006.08.040

Nomenclature

a	lateral aspect ratio
c	specific heat
C	dimensionless form-drag constant
F	Forchheimer number
g	gravity acceleration
H	height of layer
k	dimensionless wave number in the main flow direction
k_c^*	critical wave number at the double bifurcation point
k_{stg}	effective stagnant thermal conductivity
K	permeability
m	number of rolls
p	small perturbation of the pressure
P	pressure
Pe	Péclet number
Pe^*	Péclet number at the double bifurcation point
Ra	Darcy-Rayleigh number
Ra^*	Darcy-Rayleigh number at the double bifurcation point
Re_K	Reynolds number based on the permeability of the porous medium
Re_K^*	critical Reynolds number at the double bifurcation point
t	time
T	dimensionless temperature
T_0, T_1	temperature of the heated and the cooled surfaces, respectively
T^*	dimensional period of transverse modes oscillations
u, v, w	velocity components
U	dimensional average filtration velocity
V_φ	phase velocity
x, y, z	cartesian coordinates

Greek symbols

α	volumetric coefficient of thermal expansion
θ	perturbation of temperature
λ^*	dimensional wavelength
μ	dynamic viscosity
ν	kinematic viscosity
ρ	density
Φ	porosity
ω	dimensionless frequency

Superscripts

A	value of a quantity at the threshold of absolute instability
3D	transverse modes
$\|\|$	longitudinal rolls

Subscripts

b	basic solution
c	critical quantity
exp	experimental quantity
f	fluid
i	imaginary part
r	real part
s	solid
th	theoretical quantity

For porous media, which are of major importance in many natural and practical applications (see for example the book of Nield and Bejan [7]), the mixed convection problem has received very much less attention in the published literature. Moreover, compared with existing analytical and numerical works, experimental results are very limited. Almost thirty years ago, Combarnous [8–10] examined experimentally the secondary flow configurations of convection in a rectangular duct filled with a saturated porous medium through which an axial flow is maintained. The temperature recordings indicated that these configurations depend on the filtration Rayleigh number Ra and the Péclet number Pe which measures the strength of the through-flow. By using various combinations of solid particles and fluids, Combarnous obtained the flow regime map for different vortex patterns observed in experiments. Experimental evidence was given that the presence of the through-flow has no influence, neither for conduction ($Ra < 40$) nor for fluctuating flow ($Ra > 260$). For Ra between 40 and 260, depending on Pe, two main types of convective flow were observed. For low Pe the vortex flow patterns which are termed T modes in what follows are down-stream moving pure T rolls or oblique rolls. While for higher values of Pe the moving T modes are replaced by stationary L rolls. Some temperature recordings have shown that there are hysteresis effects associated with these two types of secondary flows, while other measurements have also demonstrated the coexistence of L rolls and T modes, albeit in different parts of the medium. Concerning the mean heat transfer, these experimental investigations revealed that the existence of a horizontal through-flow does not appreciably modify the vertical mean heat transfer compared with natural convection.

From a theoretical point of view, Prats [11] analyzed the linear stability of two-dimensional mixed convection in porous media of infinite lateral extension. Under the Darcy model, he showed that the critical values of the onset of mixed convection are the same as that corresponding to the onset of Horton–Rogers–Lapwood convection in an initially, quiescent fluid layer heated from below. Rees [12] extended this analysis by taking into account inertial effects as modelled by Forchheimer's correction to Darcy's law. He found that under both effects of inertia and the through-flow, L rolls are favored whatever the values of

Pe. On the other hand, by using the propagation theory in a recent paper, Chung et al. [13] obtained the critical position x_c to mark onset of L rolls. Although dominant L rolls were clearly evidenced in [12] and some of their quantitative characteristics were obtained in [13], these interesting theoretical predictions cannot be used to understand the experimentally observed moving T modes in [8–10]. As for the numerical point of view, Dufour and Néel [14] describe the two-dimensional convective configurations by focusing on the moderate values of the through-flow which correspond to the Darcian case. They computed the global frequency of oscillations, the wavelength and the phase velocity of T rolls. Recently the work of Rees has itself been extended by Delache et al. [15] to include the effects of the lateral aspect ratio of the medium in addition to the effects of the porous inertia. The pattern selection predicted by this analysis for a finite aspect ratio a is ruled by the modified Reynolds number Re_K based on the permeability of the medium. Precisely, it is found that there exists a critical Reynolds number Re_K^* at which the critical Rayleigh numbers Ra_c^{3D}, for the onset of moving T modes, and $Ra_c^{\|}$, for the onset of stationary L rolls, are equal ($Ra_c^{3D} = Ra_c^{\|}$). For $Re_K < Re_K^*$ the T modes become unstable first at Ra_c^{3D}. While for $Re > Re_K^*$ the most unstable disturbances are L rolls ($Ra_c^{\|} < Ra_c^{3D}$). Although these predictions seem to agree qualitatively with experimental results, a close inspection carried out in the present paper showed a profound disagreement. We concluded that a temporal description in the linear stability analysis is not adequate to describe such flows. Mixed flows convection belongs indeed to the open flow class such as jets and boundary layers where fluid particles continuously enter and leave the experimental medium. Therefore, the necessity of the distinction between the two types of instability, absolute or convective, is needed. In the convectively unstable regime a spatially localized perturbation is convected downstream and eventually is blown out of the system. On the contrary, in the absolutely unstable regime, such perturbations expand in the downstream as well as in the upstream direction. The behavior of the system is thus qualitatively very different in both regimes. In the convectively unstable regime, noise is spatially amplified and gives rise to noise-sustained structures. While, in the absolutely unstable regime, structures are intrinsically sustained by the deterministic dynamics.

The aim of this study is threefold. Firstly, we perform a spatio-temporal stability analysis to discriminate between the convective and absolute instability of the basic flow with respect to oscillatory three-dimensional structures as well as to longitudinal rolls. Special emphasis is given to the influence of inertia and the lateral aspect ratio of the porous medium on the instability characteristics. Secondly, the theoretical predictions are compared to experiments [8–10] conducted with various combinations of solid matrix and fluids, and hence with different ratios of the fluid thermal conductivity to the solid thermal conductivity. The predicted results are then used to verify the validity of our model based on the assumption of local thermal equilibrium between solid matrix and fluid. Finally each time possible, similarities and differences between mixed convection in porous media and in fluid media are presented.

The full nonlinear stability analysis is out of the scope of this paper.

2. Problem formulation and dispersion relation

The configuration of interest is an isotropic and homogeneous porous layer of infinite horizontal extent of rectangular cross section with thickness H and width aH saturated by a fluid. We suppose that the layer is confined by impermeable and perfectly heat conducting horizontal boundaries. The lower and upper boundaries are at uniform temperatures T_0 and $T_1 (< T_0)$. The lateral boundaries are assumed impermeable and perfectly heat insulating. Furthermore, we consider that a through-flow is driven by a pressure gradient in the x-direction. To simplify the analysis, the following conventional assumptions are applied: (1) the fluid and the porous solid matrix are in local thermal equilibrium; (2) the Forchheimer correction to Darcy's law is used for high through-flow rates or high permeability in the porous medium; and (3) the Boussinesq approximation is employed. We choose H, $H^2(\rho c)/k_{stg}$, $T_0 - T_1$, $k_{stg}/(H(\rho c)_f)$ and $k_{stg}\mu/(K(\rho c)_f)$ as references for length, time, temperature, filtration velocity and pressure. Here, k_{stg}, (ρc), $(\rho c)_f$, K and μ are, respectively, the effective stagnant thermal conductivity, the overall heat capacity of the medium per unit volume, the heat capacity per unit volume of the fluid alone, the permeability of the medium and the viscosity of the fluid. The following set of governing equations is obtained:

$$\begin{aligned} &\vec{\nabla}\cdot\vec{V} = 0 \\ &\vec{V} + F\|\vec{V}\|\vec{V} = -\vec{\nabla}P + RaT\vec{e}_z \\ &\partial T/\partial t = -\vec{V}\cdot\vec{\nabla}T + \vec{\nabla}^2 T \end{aligned} \tag{1}$$

with the following boundary conditions:

$$\vec{V}\cdot\vec{e}_z = 0 \quad \text{at } z = 0, 1; \quad \vec{V}\cdot\vec{e}_y = 0 \quad \text{at } y = 0, a \tag{2}$$

$$T = 1 \quad \text{at } z = 0;\ T = 0 \text{ at } z = 1;\ \partial T/\partial y = 0 \quad \text{at } y = 0, a \tag{3}$$

and the imposed through-flow

$$\int_0^a \int_0^1 \vec{V}\cdot\vec{e}_x \,\mathrm{d}y\,\mathrm{d}z = aPe \tag{4}$$

P, $\vec{V}$, T, $\vec{e}_z$ are the pressure, the filtration velocity, the temperature and the vertical upwards unit vector respectively. The system is characterized by four dimensionless control parameters. The filtration Rayleigh number $Ra = Kg\alpha H(T_0 - T_1)(\rho c)_f/k_{stg}\nu$, the Péclet number $Pe = UH(\rho c)_f/k_{stg}$, the number $F = C\left[K^{\frac{1}{2}}k_{stg}/H\nu(\rho c)_f\right]$ which can be termed the Forchheimer number and the lateral

aspect ratio a. U, g, ν, α and C are the average filtration velocity imposed at the entrance of the channel, the gravitational acceleration, the kinematic viscosity, the thermal expansion coefficient and a dimensionless form-drag constant, respectively.

A basic solution of the problem (1)–(4) is a combination of a vertical thermal stratification and a homogeneous flow in the $\vec{e}_x$ direction

$$\vec{V}_b = Pe \cdot \vec{e}_x,\ T_b = 1 - z \quad \text{and}$$
$$P_b = Ra(z - z^2/2) - Pe(1 + Re_K)x \tag{5}$$

where $Re_K = FPe = c\left(UK^{\frac{1}{2}}/\nu\right)$ is a Reynolds number based on the permeability of the medium. The Darcy model is recovered if $Re_K = 0$ (i.e. $F = 0$).

To investigate the stability of the basic solution (5), infinitesimal three-dimensional general perturbations are super-imposed onto the basic solution:

$$(\vec{V}, T, P) = (\vec{V}_b + \vec{v}(x,y,z,t), T_b + \theta(x,y,z,t), P_b + p(x,y,z,t)) \tag{6}$$

Substituting Eq. (6) into (1), subtracting the basic flow quantities and linearizing the equations by neglecting terms higher in order than the first one in the disturbance quantities, one can obtain the following equations for the disturbances:

$$\begin{aligned} &\partial u/\partial x + \partial v/\partial y + \partial w/\partial z = 0 \\ &u(1 + 2Re_K) + \partial p/\partial x = 0 \\ &v(1 + Re_K) + \partial p/\partial y = 0 \\ &w(1 + Re_K) + \partial p/\partial z - Ra\theta = 0 \\ &\partial\theta/\partial t - \vec{\nabla}^2\theta - w + Pe\partial\theta/\partial x = 0 \end{aligned} \tag{7}$$

Next, the three-dimensional disturbance quantities respecting the boundary conditions (2) and (3) are expressed as

$$\begin{pmatrix} u \\ v \\ w \\ \theta \\ p \end{pmatrix} = e^{i(kx-\omega t)} \begin{pmatrix} u_1 \cos[\pi z] \cos\left[\frac{m}{a}\pi y\right] \\ v_1 \cos[\pi z] \sin\left[\frac{m}{a}\pi y\right] \\ w_1 \sin[\pi z] \cos\left[\frac{m}{a}\pi y\right] \\ \theta_1 \sin[\pi z] \cos\left[\frac{m}{a}\pi y\right] \\ p_1 \cos[\pi z] \cos\left[\frac{m}{a}\pi y\right] \end{pmatrix} \tag{8}$$

where k is the wave number in the direction of the main flow, ω is the frequency and the integer m is the number of rolls in the spanwise direction. Note that we only consider solution with one roll in the vertical direction because it can be shown that the basic flow is more unstable vis-à-vis one roll than vis-à-vis multiple rolls in this direction.

If we substitute (8) into (7) we obtain an algebraic system with a nontrivial solution only if the problem is singular, which implies an explicit dispersion relation between the dimensionless parameters of the problem

$$\begin{aligned} &D(\omega, k, m/a, Ra, Pe, Re_K) \\ &= -i\omega + ikPe + k^2 + \pi^2(1 + m^2/a^2) \\ &\quad - \frac{Ra}{1 + Re_K}\left(\frac{k^2(1 + Re_K) + (m^2/a^2)\pi^2(1 + 2Re_K)}{\pi^2(1 + m^2/a^2)(1 + 2Re_K) + k^2(1 + Re_K)}\right) = 0 \end{aligned} \tag{9}$$

The following three sections are devoted to the stability analysis. Each of them corresponds to a different nature of the disturbance.

3. Temporal stability approach

Temporal stability analysis refers to the temporally growing extended perturbation in the form of a spatially homogeneous wave with a real wave number k. The temporal growth rate of unstable perturbations is given by the imaginary part of the frequency $\omega = \omega_r + i\omega_i$. Therefore, the neutral temporal stability curve is obtained for $\omega_i = 0$ which selects dominant modes at the onset of convection. This temporal stability approach has been considered by Delache et al. in a published note [15], and has provided quantitative information on the stability condition. Here, we briefly recall the main results of [15] and report some new and complementary findings.

We first study the stability of (5) against stationary L rolls (i.e., $k = 0$ and $\omega_r = 0$). For a given (finite) value of a, we found that the threshold $Ra_c^{\parallel}$ of L rolls

$$Ra_c^{\parallel} = \pi^2(a/m_{\parallel} + m_{\parallel}/a)^2(1 + Re_K) \tag{10}$$

is raised by porous inertia contrarily to the case of mixed convection in a fluid medium. Indeed, the studies [4,5] of PRB flows reported that $Ra_c^{\parallel}$ is independent of Reynolds number. The variations of $Ra_c^{\parallel}/(1 + Re_K)$ versus a are depicted in Fig. 1. We also indicate the number m of L rolls, which depends on a. Notice that for integer values of a, $Ra_c^{\parallel} = 4\pi^2(1 + Re_K)$ and $m = a$. Otherwise the lateral confinement stabilizes the basic flow against the L rolls and the maximum of $Ra_c^{\parallel}$ decreases when a is increased and tends to $4\pi^2(1 + Re_K)$ when lateral boundaries are pulled to infinity, in agreement with [12]. We note that the stabilizing effect of lateral walls is more important in clear fluids [4] than in porous media. This observation stems from the fact that the values of the ratio $(Ra_c^{\parallel}(a) - Ra_c^{\parallel}(a \to \infty))/Ra_c^{\parallel}(a \to \infty)$, where $Ra_c^{\parallel}(a)$ is the threshold with a finite a, are always larger in fluid media (see Fig. 7 of [4]) than in porous ones (Fig. 1).

Oscillatory three-dimensional instabilities (T modes) are characterized by non-zero values of k, ω_r and m. The corresponding threshold Ra_c^{3D} is given by

$$Ra_c^{3D} = \left(\sqrt{1 + Re_K(1 - m_{3D}^2/a^2)} + \sqrt{1 + 2Re_K}\right)^2 \pi^2 \tag{11}$$

with m_{3D} being the largest integer m satisfying

$$m^2/a^2 < (1 + Re_K)/(1 + 2Re_K) \leqslant 1 \tag{12}$$

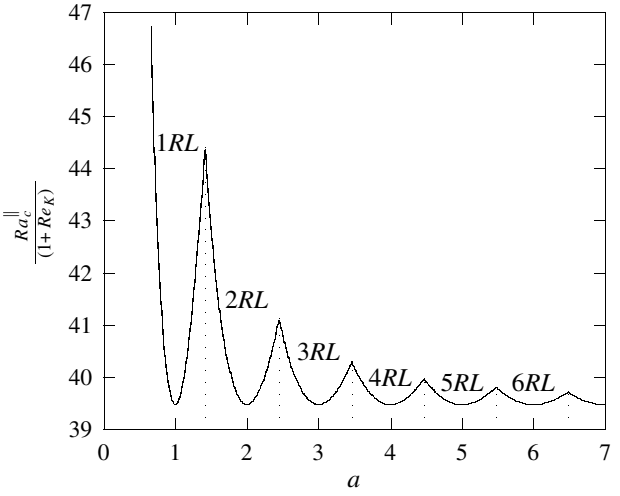

Fig. 1. Critical threshold (normalized by $1 + Re_K$) of the appearance of longitudinal rolls and their number as a function of transversal aspect ratio a.

The oscillation frequency is $\omega_r = k_c Pe$ with the critical wave-number k_c defined as

$$k_c^2 = \frac{\pi^2\left[-(m_{3D}^2/a^2)(1+2Re_K) + \sqrt{(1+2Re_K)(1+Re_K(1-m_{3D}^2/a^2))}\right]}{1+Re_K} \tag{13}$$

From the comparison between $Ra_c^{\parallel}$ and Ra_c^{3D}, some conclusions may be drawn.

First, when a is not an integer and is larger than 1, it is found that there exists a critical Reynolds number Re_K^* below which the T modes propagating with a phase velocity equal to Pe become unstable first at Ra_c^{3D}. While for $Re > Re_K^*$ the most unstable disturbances are L rolls ($Ra_c^{\parallel} < Ra_c^{3D}$). A transition occurs between T modes and L rolls at Re_K^* for which the critical Rayleigh numbers, Ra_c^{3D} and $Ra_c^{\parallel}$ are equal (i.e. $Ra_c^{3D} = Ra_c^{\parallel} = Ra^*$). This

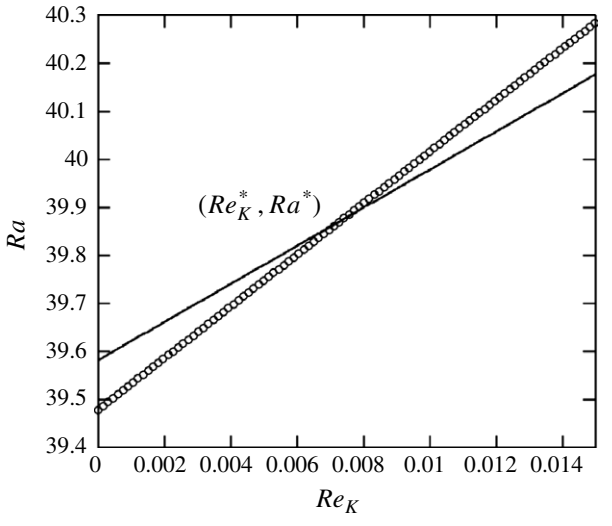

Fig. 2. Critical threshold of both 3D oscillatory structures (○) and L rolls (—) as a function of Re_K for $a = 1.9$.

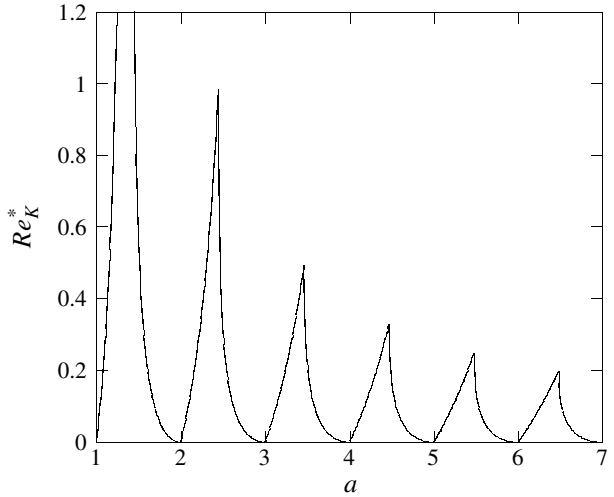

Fig. 3. Values of Re_K^* for which $Ra_c^{3D} = Ra_c^{\parallel}$ as a function of a.

behavior is represented in Fig. 2. The dependence of Re_K^* on the lateral aspect ratio is also displayed in Fig. 3. In what follows, the point (Re_K^*, Ra^*) will be termed a double bifurcation point. Second, for infinite or integer values of a, the lowest threshold corresponds to L rolls which then dominate whatever the values of Re_K.

Finally, we examined the way by which the predicted transition from T modes to L rolls occurs at the double bifurcation point. We evaluated the wave number k_c^* at this point for different values of the aspect ratio a and found that this transition may be smooth or abrupt depending on a. As shown in Fig. 4, for $a \in]E(a), \sqrt{a(a+1)}]$ and $E(a)$ the entire part of a, we obtain $m_{\parallel} = m_{3D} = E(a)$ and $k_c^* = 0$. Therefore, we expect that the system may exhibit a smooth transition from T modes to L rolls. On the contrary, for $a \in [\sqrt{a(a+1)}, E(a)+1[$, we find $m_{3D} = E(a)$, $m_{\parallel} = E(a)+1$ and $k_c^* \neq 0$ implying that this transition is abrupt. From the phenomenological standpoint, there is

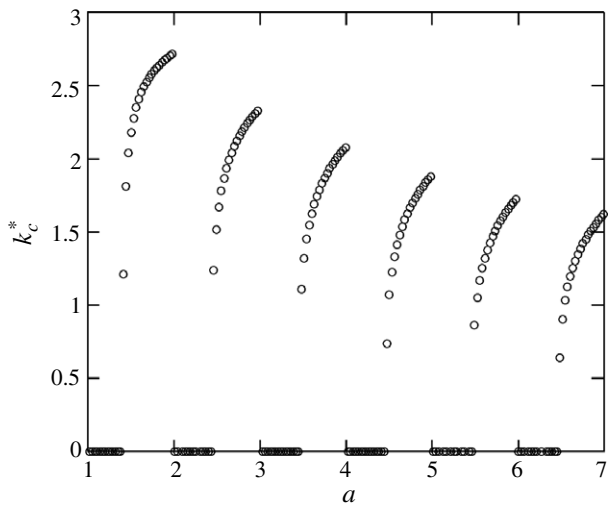

Fig. 4. Critical wave number k_c^* for which $Ra_c^{3D} = Ra_c^{\parallel}$ versus a.

a fairly close analogy between the abrupt or smooth transition described above and the transition predicted by Rees and Postelnecu [17] in their analysis of a completely different problem, namely the onset of convection in an inclined anisotropic porous layer. They concluded that there is not a straightforward exchange between T rolls and L rolls, but rather the transition may be smooth or abrupt depending on the anisotropy of the medium.

4. Spatial stability approach and transition to absolute instability

4.1. 3D Oscillatory patterns

Comparing experimental measurements with the temporal stability predictions, we found a deep discrepancy (see Section 6). We concluded that a temporal description in the linear stability analysis is not adequate to describe mixed convection flows. The spatial theory is then used: in contrast to a temporal stability analysis, a forcing perturbation imposed at a specific location in the fluid, say $x = 0$, is not allowed to grow in time (i.e. $\omega_i = 0$), but it can grow in space. Therefore k is a complex number: $k = k_r + ik_i$. Its real part k_r represents the wave number; the opposite of its imaginary part $-k_i$ represents the spatial growth rate, and the real number ω gives the frequency of the wave. Hence unstable waves propagating in the through-flow direction are such that $-k_i > 0$.

The spatial branches for oscillatory three-dimensional patterns are defined by

$$\Gamma = \{k \in \mathbb{C}, \omega \in \Re / D(k, \omega, Ra, Pe, F, m/a) = 0\} \tag{14}$$

$D(k,\omega,Ra,Pe,F,m/a) = 0$ is the dispersion relation (9) which we expand to obtain a fourth-degree polynomial of k. We numerically solve it and obtain the four spatial branches of (14) for different values of Ra and fixed values of Pe, F and m/a. The four branches are plotted in the complex k plane in Fig. 5(b)–(d), for different Ra. The spatial branches corresponding to waves propagating in the through-flow direction (i.e. $x > 0$) are denoted by k^+. Similarly, k^- branches are associated to waves moving in the upstream direction (i.e. $x < 0$). In order to discriminate between k^+ and k^- in the complex k plane, we proceed as it follows. For $Ra < Ra_c$, the system is stable and all temporal modes (i.e. k real and ω complex) lie under the real k-axis as it is shown by the circle line of Fig. 5(a), meaning that no ω real and k real is solution of the dispersion equation. Therefore, spatial branches do not cross the real k-axis (Fig. 5(b)) and lie on each side of it. As the basic state is stable, any wave propagating downstream or upstream is not allowed to grow spatially and must be damped. Thus branches with $k_i > 0$ ($k_i < 0$) shall be associated to $k^+(k^-)$. When Ra exceeds slightly Ra_c, the basic flow is destabilized and the temporal branch crosses over the real k-axis as it is shown by the solid line of Fig. 5(a). Intersection of this temporal branch with $\omega_i = 0$ gives a wave pertaining to a spatial branch as well. Therefore k^+ crosses the real k-axis (Fig. 5(c)) and then the amplitude of the wave packet corresponding to the selected frequency ω will increase downstream ($-k_i^+ > 0$) and will decrease upstream ($-k_i^- < 0$). Moreover, as it is shown in Fig. 5(e) and (a) large band of frequencies may emerge in the medium which imply that the system acts as a spatial amplifier of the inlet perturbation. This is the main characteristic of the convective instability. As the Rayleigh number is increased, the maximum spatial growth rate increases, and the peak of the frequency spectrum becomes less broadened. Increasing the Rayleigh number to a threshold, $Ra = Ra^A$, the spatial growth rate presents a cusp point at the frequency $\omega = \omega^A$ as it is illustrated in Fig. 5(f). Moreover, for this value of the Rayleigh number, two branches emerge from the lower and from the upper half-planes, pinch below the real wavevector axis at ω^A and create a saddle-point (Fig. 5(d)). Owing to the symmetry (k_r, k_i, ω) → ($-k_r$, k_i, $-\omega$) of the dispersion equation, the pinching process occurs symmetrically with respect to $k_r = 0$ axis. This is the so-called pinching condition, necessary and sufficient for the onset of the absolute instability (see, for instance the review of Huerre and Monkewitz [18]). It is important to note that at the threshold of the absolute instability, no distinction can be made between the two spatial branches k^+ and k^- which coalesce at the saddle-point. For this reason, the response of the system to an inlet forcing can not be defined implying that the flow behaves as a self-excited oscillator with intrinsic dynamics. The values of the Rayleigh number, the wave number and the frequency at the saddle point, (Ra^A, k^A, ω^A), for fixed values of m/a, Pe and F, are called the absolute Rayleigh number, the absolute wave number and the absolute frequency, respectively. In the following we present results related to the border between convective and absolute instability.

To investigate the roll orientation corresponding to the highest absolute growth rate, we use the spatial stability approach described above by considering general oscillatory three-dimensional mode. For $a = 6.9$, that is the lateral aspect ratio used in experiments [8–10] and according to relation (12), the unstable modes correspond to values of m ranging from 0 to 6. The dependence on the Péclet number of Ra^A is determined for different m. We found that Ra^A raises with increasing m for all Pe numbers. Therefore, the mode $m = 0$ is the first to be absolutely unstable and we therefore conclude that the boundary of absolute instability coincides with that of oscillatory pure transverse rolls. We have checked that this pattern selection related to the border between convective and absolute instability remains pertinent for any Forchheimer number F. Fig. 6 displays the absolute threshold Ra^A versus Pe for the modes $m = 0$ and $m = 6$ with $F = 0$ (i.e. under the Darcy model). The curves of the absolute threshold for the remaining unstable modes with $1 \leqslant m \leqslant 5$ lie between the depicted ones.

The influence of inertia on the boundary between convective and absolute instability for pure transverse rolls is investigated by varying the Forchheimer number F. It is shown in Fig. 7(a) that Ra^A ($m = 0$) increases when F

increases meaning that the basic flow is less absolutely unstable with respect to T rolls when F is raised. Explaining the physical reasons behind this phenomenon requires to interpret this result in terms of the product, $FPe = Re_K$ which represents the ratio of inertia to viscous terms. The increase of Re_K (i.e. the increase of inertia effects) is accompanied by a stabilization of the flow. For example, if we take $Pe = 10$ and change F from 0 to 0.01 and then to 0.1, the threshold of the absolute instability raises from 58 to 66 and to 142 respectively. We claim that these predictions, compared to experimental results in thin porous layer and in high-porosity media where inertial effects are

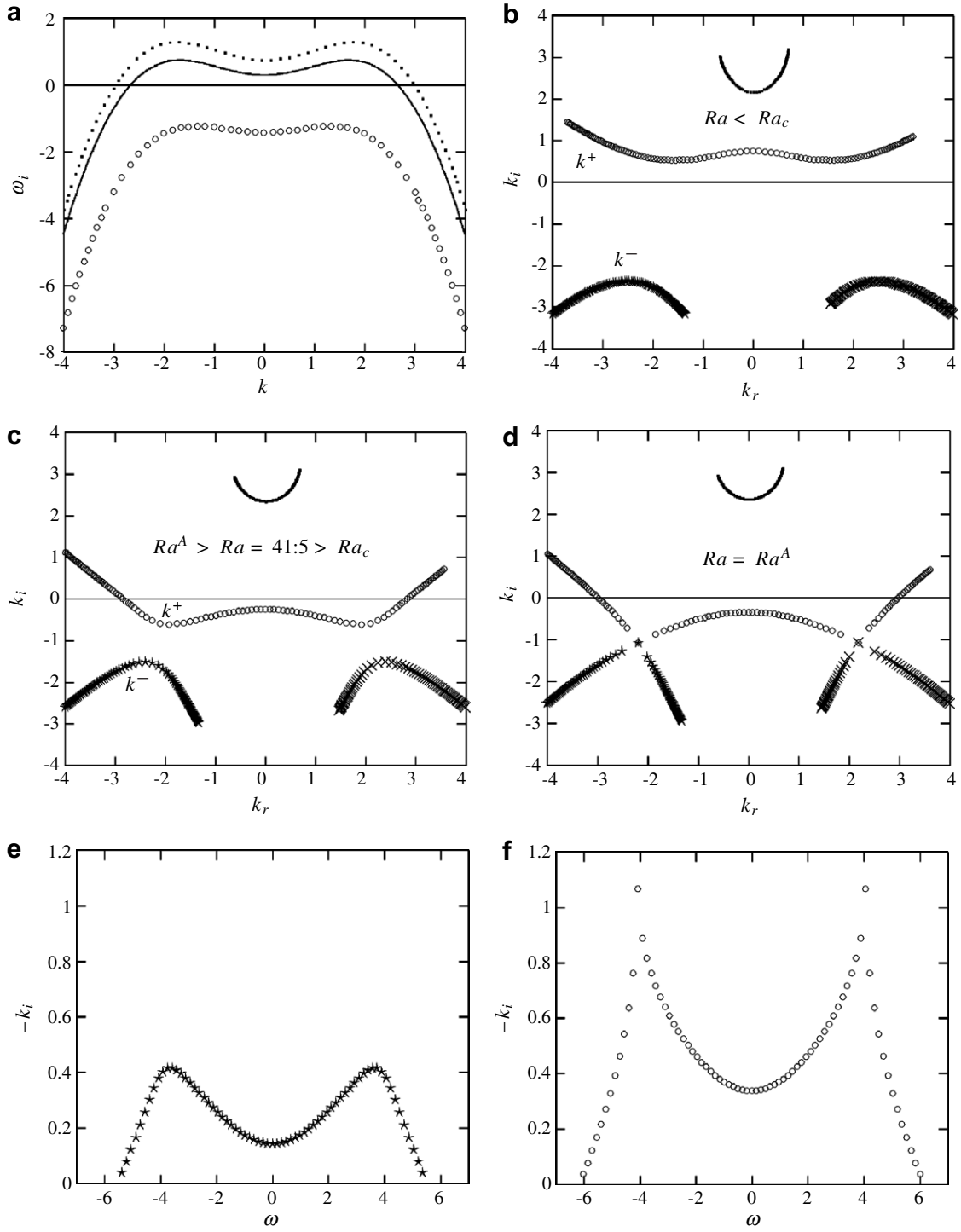

Fig. 5. (a) Temporal rate ω_i versus k real for $Ra = 37 < Ra_c$ (○), $Ra = 41.5 > Ra_c$ (—) and $Ra = Ra^A = 42$ (···); (b)–(d) spatial branches in the (k_r, k_i) plane at stable case $Ra = 37$ (b), at convectively unstable case $Ra = 41.5$ (c), at the threshold of the absolute instability $Ra = 42$ (d); ($-k_i$) versus ω for $Ra = 41.5$ (e) and for $Ra = 42$ (f). Here $Pe = 2$ and $m = 6$, $a = 6.9$.

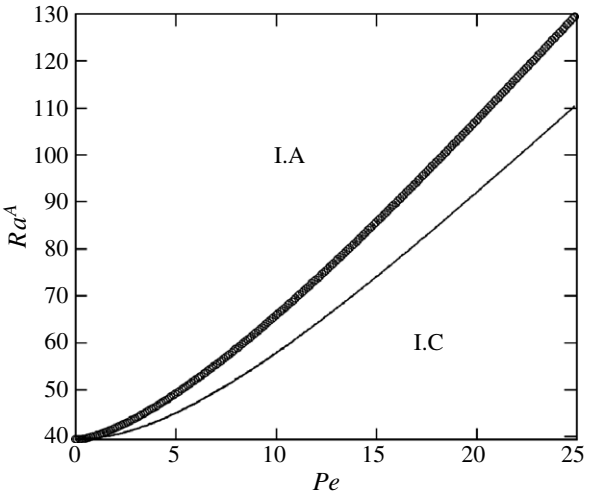

Fig. 6. Boundaries between convective (IC) and absolute (IA) instability for T modes in the (Pe, Ra) plane for $F = 0$. The lower and the upper curves correspond to $m = 0$ and 6.

significant may be used to test the Forchheimer model as a nonlinear correction to Darcy's law.

Some characteristics of T rolls in the boundary between convective and absolute instability, namely the oscillation frequency ω^A, the wave number k_r^A and the phase velocity $V_\varphi^A = \omega^A/k_r^A$ are expressed as a function of Pe for $F = 0$, 0.01 and 0.1 and are displayed in Fig. 7(b)–(d). The illustrations indicate that inertia have weakly effects on the three characteristics. Moreover, the phase velocity V_φ^A is almost equal to Pe irrespective of F.

4.2. Longitudinal rolls

Before considering the influence of a finite lateral aspect ratio a on the convective or absolute nature of the instability for L rolls, it should be emphasized that the present work, in the limit of infinite a, has close similarities with previous studies published on the Poiseuille–Rayleigh–Bénard (PRB) problem [5] and on mixed convection of binary mixtures in porous media [19,20]. In both problems, the authors performed a spatio-temporal analysis by evaluating the asymptotic response to localized 3D perturbations. As far as the width of the medium is assumed infinite, these studies revealed that in the absolute instability region, the

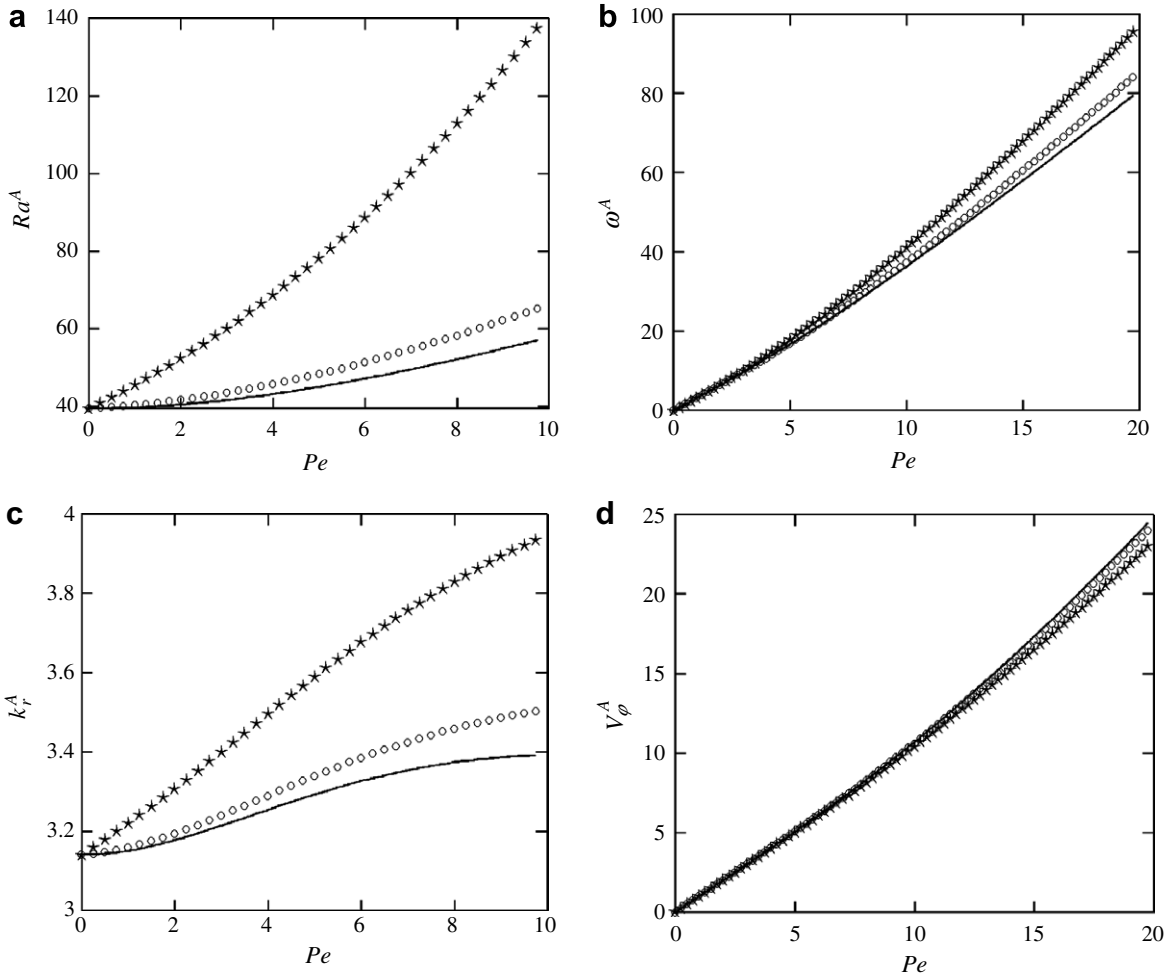

Fig. 7. Characteristics of T rolls at the threshold of the absolute instability for different Forchheimer numbers $F = 0$ (—), $F = 0.01$ (○) and $F = 0.1$ (★) (a): $Ra^A(Pe)$, (b): $\omega^A(Pe)$, (c): $k_r^A(Pe)$ and (d): $V_\varphi^A(Pe)$.

system selects pure travelling T rolls while the system remains convectively unstable with respect to oblique T modes as well as to L rolls for all non-zero through-flow values. As pointed out in [5], the result that L rolls represent a convective instability for all non vanishing Reynolds numbers in PRB problem is in contradiction with the prediction of amplitude equations derived by Brand et al. [21], Müller et al. [22] and Tveitereid and Müller [23], who found that L rolls may experience a transition to absolute instability in some parameter ranges. The authors of [5] attributed this result to the fact that amplitude equations were used outside their range of validity. Recently, in the limit of very low Reynolds number, Carrière et al. [24] rigorously derived an amplitude equation describing the dynamics of any instability with arbitrary orientation in PRB problem. The main result obtained from this amplitude equation is that all instability modes (including L rolls) are convectively unstable except pure T rolls in agreement with [5]. In this subsection, we try to throw a new light on this subject by considering the influence of the lateral confinement of a porous medium on the nature of the instability for L rolls.

One of the key differences between an infinite and a finite lateral aspect ratio regarding the stability problem lies in the property of the wave number in the y-direction. In the case of an infinite extension the wave-number is continuous. The presence of lateral walls selects discrete values of the wave-number rather than continuous values. Consequently in the former case we obtain a continuous neutral stability curve, while in the later case the spectrum of growth rates is discrete. In Section 3, we found that the growth rate of L rolls vanishes if $Ra^{\|} = \pi^2(a/m + m/a)^2(1 + Re_K)$. For a given (finite) value of a, the threshold $Ra_c^{\|}$ is obtained for a number of rolls $m_{\|}$ which minimizes $Ra^{\|}$. The remaining modes with $m \neq m_{\|}$ are less unstable. Nevertheless in the following, we will try to locate a possible transition from convective to absolute instability for the most unstable $m_{\|}$ mode as well as for the others m modes. To find possible saddle points we pursued the same procedure as described above for oscillatory three-dimensional patterns. For example, the pinching process of spatial branches for varying Ra is illustrated in Fig. 8(a) for $a = 6.9$ and $m = 8$. As may be seen from this figure, the saddle point is located along the imaginary k_i-axis, meaning that the dominant mode is L rolls. We have checked that this feature is also observed for different finite a, including integer values of a. We did not find any similar pinching process for infinite a or finite a with $m < m_{\|}$ meaning that in this case L rolls remain convectively unstable whatever Péclet number. Fig. 8(b) displays in the (Pe, Ra) plane the transition curve to absolute instability of L rolls for $a = 6.9$ and different m satisfying $m \geqslant m_{\|}$. A remarkable feature is that L rolls can be absolutely unstable only if the Péclet number Pe is less than a critical value $Pe^c(m)$ which increases with increasing m. As Pe exceeds $Pe^c(m)$ the threshold of the absolute instability tends to infinity.

5. Instability characteristics in the absolutely unstable regime

The temporal stability analysis given above refers to the case of extended perturbations and considers a complex frequency, ($\omega = \omega_r + i\omega_i$), for known real wave number, ($k_i = 0$). On the other hand, a spatial stability analysis considers the response of the system to a localized harmonic forcing where the complex wave number, ($k = k_r + ik_i$), has to be found for known real frequency values, $\omega_i = 0$. The spatial stability analysis is not adequate if Ra exceeds Ra^A. Therefore, the most general case in which the initial impulse response at a fixed spatial location is evaluated by considering both the complex frequency and the complex wave number must be considered. For the sake of brevity, we formally describe the method and state the results here and the reader should consult reference [16]

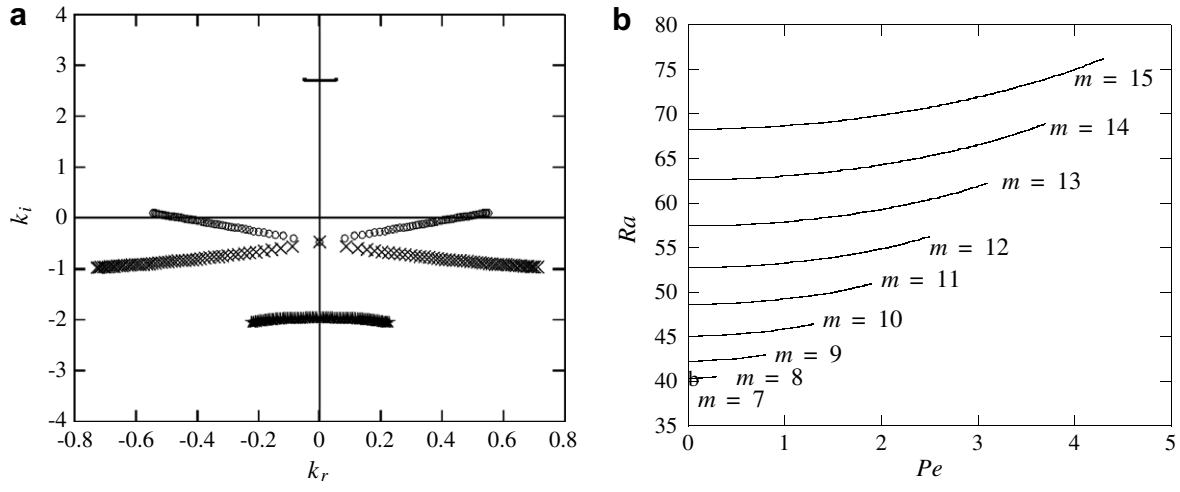

Fig. 8. (a) Pinching of spatial branches of L rolls for $Pe = 0.225$, $a = 6.9$, $m = 8$ and $Ra = 40.41$. (b) Transition curves to absolute instability for L rolls in the (Pe, Ra) plane with $m = 7, 8, \ldots, 15$.

for technical details. The classical method consists to add to the right-hand side of the system (7) a localized initial impulse in (x, y, z) space for $G=(u,v,w,p,\theta,)^{\mathrm{T}}$ (i.e. the Green function). The problem can be solved using Fourier transform in space and Laplace transform in time, defined by:

$$\widehat{G}(k,\omega,y,z)=\int_{-\infty}^{\infty}\int_{0}^{\infty}G(x,y,z,t)\exp(\mathrm{i}(\omega t-kx))\,\mathrm{d}x\,\mathrm{d}t \tag{15}$$

By solving the problem in Fourier space and performing the Laplace transform by residue theorem, the solution $G(x,y,z,t)$ may be written formally as

$$G(x,y,z,t)=-\frac{i}{2\pi}\int_{-\infty}^{\infty}\frac{S(k,\omega,y,z)}{\frac{\partial D}{\partial\omega}(k,\omega)}\exp(-\mathrm{i}(\omega t-kx))\mathrm{d}k \tag{16}$$

Here $S(k,\omega,y,z)$ depends on the shape of localized initial impulse.

The asymptotic behavior of the integral (16) can be obtained by applying the method of the steepest descent [18]. The dominant part of the integrand arises in the region of the complex saddle point k^{s} defined by

$$\mathrm{d}\omega/\mathrm{d}k=x/t \tag{17}$$

In the unstable regime, localized perturbations expand in the form of wave packets with the growth rate $\sigma=\omega_{\mathrm{i}}-k_{\mathrm{i}}x/t$. Besides the temporal growth rate ω_{i}, σ is also composed of a spatial contribution term where the propagation velocity $U=x/t$ of the wave packet plays a key role.

In case of temporal instability analysis, the system is unstable provided that $\omega_{\mathrm{i}}>0$ for any real wave number, and the most unstable wave number k_{c} is defined by $\mathrm{d}\omega_{\mathrm{i}}/\mathrm{d}k=0$. The ray direction along which the maximum growth rate is reached is defined by $(\mathrm{d}\omega_{\mathrm{r}}/\mathrm{d}k)_{\mathrm{c}}=(x/t)_{\max}$.

The second parameter domain of special interest concerning spatio-temporal instabilities, is that corresponding to a maximum growth rate for a given x as $t\to\infty$ that is $x/t\to 0$. The complex wave number k_0 associated with this instability satisfies the equation $\mathrm{d}\omega/\mathrm{d}k=0$. Thus, a perturbation at fixed x grows with a rate $\omega_{\mathrm{i}}(k_0)$. When $\omega_{\mathrm{i}}(k_0)$ is positive, the system is said to be absolutely unstable and localized perturbations grow in situ and also expand in space. If $\omega_{\mathrm{i}}(k_0)$ is negative, $\omega_{\mathrm{i}}(k_{\mathrm{c}})$ being positive, the system is said to be convectively unstable meaning that any localized impulse is convected away so that instabilities cannot globally grow.

In order to determine the main characteristics beyond the threshold of absolute instability (i.e. $\omega_{\mathrm{i}}(k_0)>0$), the following system is solved by means of a Newton–Raphson algorithm

$$D(\omega,k_0,m/a,Ra,Pe,F)=0\quad\text{and}\quad\mathrm{d}\omega/\mathrm{d}k=0 \tag{18}$$

The first expression in (18) is the dispersion relation, and the second equation expresses the existence of a saddle point in the complex wave number plane, i.e. the nullity of the complex group velocity.

An interesting issue is the evolution of the wavelength, the period of oscillations and the phase velocity of the most absolutely unstable pattern, namely the oscillatory pure transverse rolls, with varying Ra and Pe. Fig. 9(a) demonstrates that the wavelength λ decreases with Ra for fixed Pe. The same behavior was predicted in simulations of the governing equations of mixed convection in clear fluids by Nicolas et al. [25] for Prandtl number $Pr=6.4$ and by Schröder et al. [26] for $Pr=530$ in qualitative agreement with experiments [27]. As for the variation of λ on Péclet number, Fig. 9(a) shows that for fixed Ra, λ increases for increasing Pe while the inverse is found in mixed convection in clear fluids [25–27]. Therefore, it is interesting to clarify this feature with regard to experimental results, a

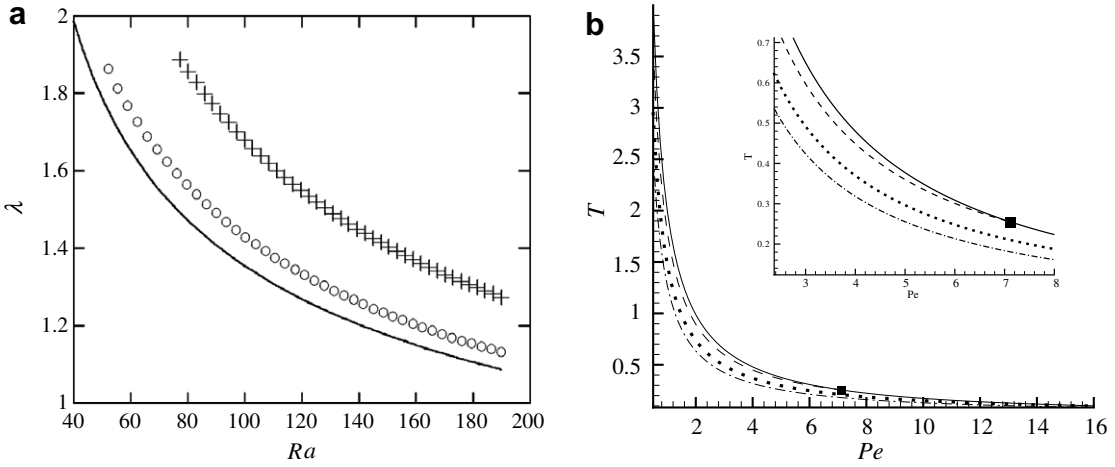

Fig. 9. Characteristics of T rolls in the absolutely unstable region: (a) wavelength versus Ra for $Pe=1$ (−), $Pe=8$ (○) and $Pe=16$ (+) (b): beside the period T^{A} at the border between convective and absolute instability (—) are represented the period of oscillations versus Pe for: $Ra=50$ (---), $Ra=80$ (···) and $Ra=120$ (- · -).

task that will be accomplished in the next section. The period T of oscillatory pure transverse rolls is plotted in Fig. 9(b) as a function of Pe for several Rayleigh numbers. This figure shows that the period T is diverging for $Pe \to 0$ regardless of Ra, in agreement with the zero frequency at marginal stability of the classical Horton–Rogers–Lapwood convection. Moreover, the period T is also shown to decrease with increasing Ra for fixed values of Pe and to decrease with increasing Pe for fixed values of Ra and eventually equals the period T^{A} at the border between convective and absolute instability (see the inset of Fig. 9(b)). This is in good qualitative agreement with the results of two-dimensional numerical simulations of Dufour and Néel [14]. Finally, we found that the phase velocity V_{φ} is almost equal to Pe. Once again, this is confirmed quantitatively by the result of the numerical simulation of [14].

We conclude this section by recalling that beyond the absolute instability threshold, the three predicted features of oscillatory pure transverse rolls, namely the wavelength, the period of oscillations and the phase velocity are in qualitative agreement with the nonlinear numerical results of [14]. The aim of the next section is to go one step further by comparing these predictions with results issuing from experiments.

6. Comparison with experiments

In early experiments on mixed convection in porous media (referred as MC throughout this section) conducted by Combarnous and published in [8–10] the distinction between convective and absolute instability was not yet established. Therefore it is a useful task to examine the MC findings using the concept of absolute instability which is now widely recognized. We will focus here on the results. The details on experimental system are given in [10] for example. In MC experiments an extensive pattern of thermo-couples was set in the porous medium with a view to observe the cellular organization of convective movements. The porous media consist of various solid beads (glass, sand, lead) and fluid (water, oil) depending on the experimental series. The depth of the porous media is 5.35 cm while their width is 37 cm so as the lateral aspect ratio of the working volume is $a = 6.9$. With this lateral aspect ratio, the predicted value of Reynolds number at the double bifurcation point is $Re^{*}_{K} = F \times Pe^{*} = 1.19 \times 10^{-3}$. Table 1 presents the calculated values of Pe^{*} for the four series presented here, together with different thermo-physical properties as they have been evaluated in [8].

Selected results from MC experiments will be presented in the following to illustrate the flow patterns together with their characteristics in the laminar mixed convection region i.e. $Ra < 260$. The temperature recordings allowed to delineate a flow regime map of various patterns including a conductive state, stationary L rolls, regular and irregular moving T modes. Figs. 10 and 11 present the experimental flow regime maps in the (Pe, Ra) plane for different series. Additionally in Fig. 10 we specify the initial condition for each run. In all reported experiments, the pattern observed as a final state of a run of a number n is taken as an initial condition for the next run $n + 1$, except for the first moving T modes (i.e. number 1) which are the consequence of a conduction state as an initial condition. The missing numbers in Fig. 10 correspond to complicated patterns observed in the fluctuating mixed convection region, not studied in this work. We inform the reader that these initial conditions are not specified in [8–10]. We also present the convective/absolute instability boundaries of T rolls together with Pe^{*}, the value of Péclet number at the double bifurcation point (vertical line in Fig. 11). According to the

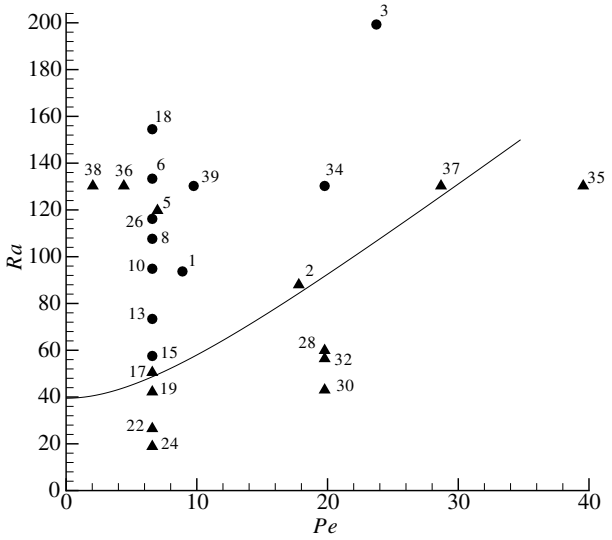

Fig. 10. Flow regime map in the (Pe, Ra) plane for patterns observed in [8] for series 6 (glass beads of diameter 4 mm/water) in laminar region: T modes (●) and L rolls (▲). Experimental runs are indicated by the numbers. The missing numbers are located in the fluctuating region. The curve represents the border between convective and absolute instability for T rolls predicted theoretically. Here $Pe^{*} = 7.65$.

Table 1
Thermo-physical properties for experimental series and corresponding values of Pe^{*}

Series	Solid/liquid	Φ	$K \times 10^{-8}$ m^2	k_s ($\times 10^{-1}$) W/m (°C)	k_f (10^{-1}) W/m (°C)	k_{stg} ($\times 10^{-1}$) W/m (°C)	Pe^{*}
6	Glass/water	0.371	1.147	1.5	0.6	0.85	6.95
7	Glass/oil	0.351	0.228	1.5	0.15	1.03	13.27
11	Glass/water	0.381	0.721	1.5	0.6	0.9	7.68
14	Quartz/water	0.324	0.209	6	0.6	4.25	3.29

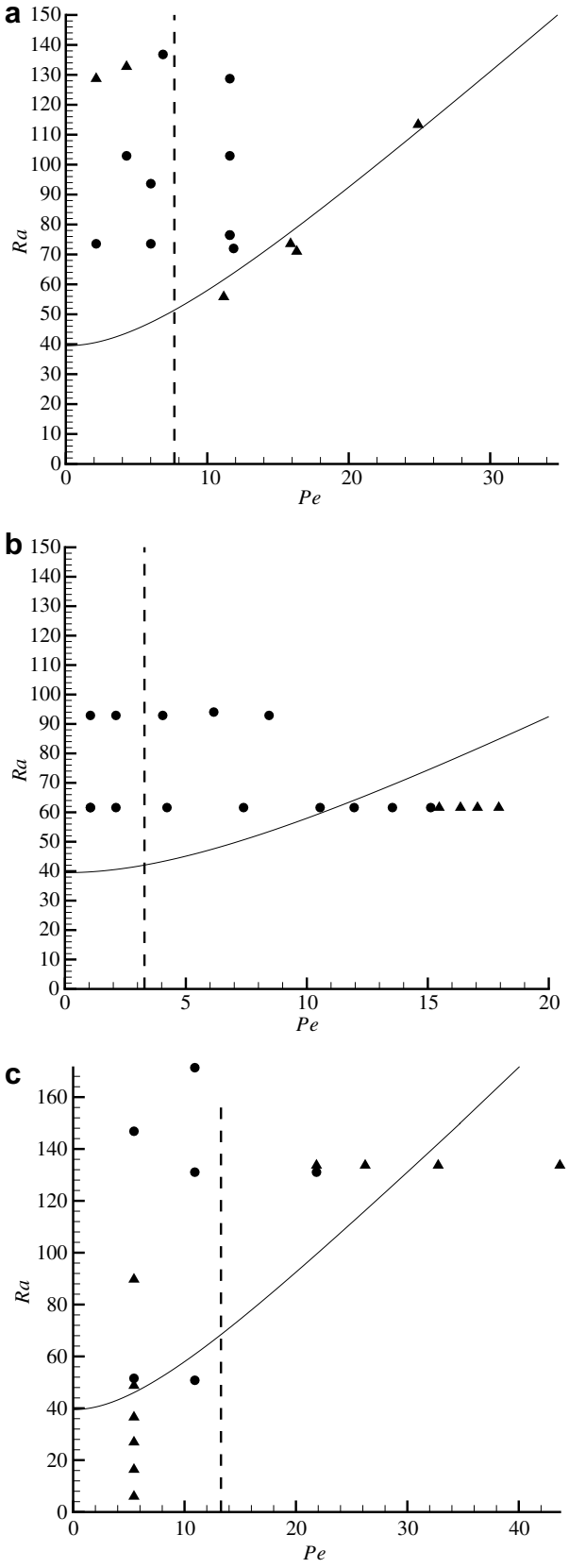

Fig. 11. Flow regime maps as in Fig. 10 for: (a) series 11 (glass beads of diameter 3 mm/water) (b) series 14 (quartz of diameter 2.25 mm/water) and (c) series 7 (glass of diameter 2 mm/oil). The vertical line represents $Pe = Pe^*$.

discussion of roll pattern selection performed in Section 3, one should observe the oscillatory three-dimensional pattern when $Pe < Pe^*$ and L rolls otherwise. This prediction stemming from the linear temporal stability analysis does not agree with experiments as shown in Figs. 10 and 11. On the other hand, for series 6 and 11, the border between convective and absolute instability of different oscillatory modes corresponds perfectly to the observed transition from either T modes or irregular patterns in turbulent regime (not shown in Figs. 10 and 11) to L rolls and conversely. Indeed, by examining the Fig. 10 we can appreciate this behavior throughout different scenario:

(i) Raising Pe for a fixed value of Ra: point 34 to point 35.
(ii) Increasing or decreasing Ra in laminar region for fixed value of Pe: point 17 to point 18 and point 18 to point 19 respectively.
(iii) Decreasing Ra from turbulent region ($Ra > 260$) for fixed value of Pe: points 27, 29 and 31 (not shown in Fig. 10) to points 28, 30 and 32 respectively.
(iv) Decreasing Ra and increasing Pe: point 1 to point 2.

Besides the results mentioned above, the MC experiments revealed the existence of a region associated with either T modes or L rolls according to the initial conditions (points 34, 36, 37, 38 and 39 of Fig. 10). We emphasize that complicated nonlinear effects are behind this pattern selection. Therefore three-dimensional numerical simulation is needed to clarify these hysteresis effects. In particular, the competition between T modes and L rolls is worth examining in the framework of a model based on coupled amplitude equations. Work in this direction is in progress. Except in parameter ranges where hysteresis effects are present, a close inspection of Figs. 10 and 11 points to the fact that the linear concept of absolute instability provides the relevant pattern selection and stability criteria. Nevertheless, problems arise for series 7 and 14 for which there is no good relation between the transition curve to the absolute instability and the observed transition between T modes and L rolls as shown in Fig. 11(b) and (c). We believe that the key explanation of the difference between experiment and theory lies in the fact that the matrix used in series 7 and 14 has a much greater thermal conductivity than that of the fluid (i.e. $k_f/k_s = 0.1$). Therefore, the assumption of local thermal equilibrium is less satisfactory and one has to include in the mathematical model the effect of finite heat transfer coefficient between the two phases [28,29].

In a recent study of nonlinear dynamics of parallel wakes, by computing the linear and nonlinear response to localized perturbations, Chomaz [30] found that nonlinear effects do not modify some of the instability characteristics. In particular, he showed that the global frequency is the absolute frequency determined by linear criteria although the system is fully nonlinear. From these encouraging results concerning an example of open flow systems, it is

interesting to compare the wavelength, the phase velocity and the period of oscillations predicted by linear theory of absolute instability to experiments.

The MC experiments exhibit a unique wavelength selection depending on Ra and Pe numbers. Fig. 12 exemplifies the spatial distribution of the temperature along the axis of the medium, i.e. at $z = 1/2$ and $y = a/2$, as it has been measured in [8] for $Ra = 72$ and $Pe = 12.25$, after asymptotic state is reached. From Fig. 12 emerge two significant points: first, the sinusoidal behavior of the temperature occurs around an average temperature of 23.5 °C and not around the temperature of the conduction state $(T_0 + T_1)/2 = 24.95$ °C as it is assumed theoretically (the discrepancy is of 5.8%); and second the longitudinal aspect ratio 61 cm/5.35 cm $\simeq$ 11.5 is not large enough and allowed the occurrence of at most six wavelengths. Understanding the influence of the above-mentioned two points on the wavelength will help in assessing the agreement between experimental and theoretical results. In the PRB flows, it was shown numerically [25,26,31] and experimentally [26,27] that the wavelength and the propagation speed of the rolls are strongly dependent on the inlet and the outlet boundaries as well as on the longitudinal aspect ratio of the medium. In particular, if instead of imposing the conduction state at inlet and outlet, and consider phase-pinning at the boundaries [31] found that the wavelength of T rolls is not uniform over the length of the box. The same behavior was also experimentally observed in PRB in the case of a short box [26]. Therefore, if we try to make quantitative comparison between theory and experiment, we have to take into account the relatively large uncertainty to measure both the wavelength and the propagation speed of T rolls in laboratory experiment. The comparison is achieved in two ways. Because the measured wavelengths were obtained for different combinations of Ra and Pe numbers, we first try to draw a main tendency of the wavelength by using a least-square approximation. The interpolation of measured wavelengths λ^*_{exp} is presented in dimensional form in Fig. 13 as a function of Ra for series 11, together with the interpolation of wavelengths of T rolls ($m = 0$) or oscillatory three-dimensional structures ($m = 6$) predicted by the linear concept of absolute instability. The wavelength curves of three-dimensional structures with

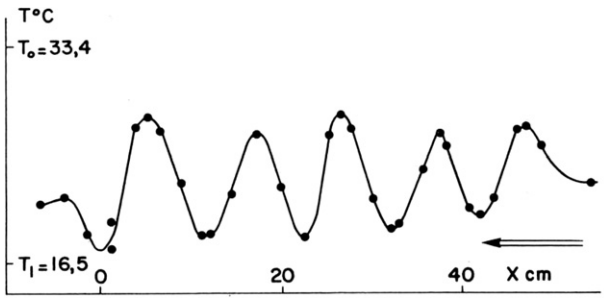

Fig. 12. Spatial distribution of the recorded temperature along the middle axis $z = \frac{1}{2}$ and $y = \frac{a}{2}$ [8]. The arrow indicates the through-flow direction.

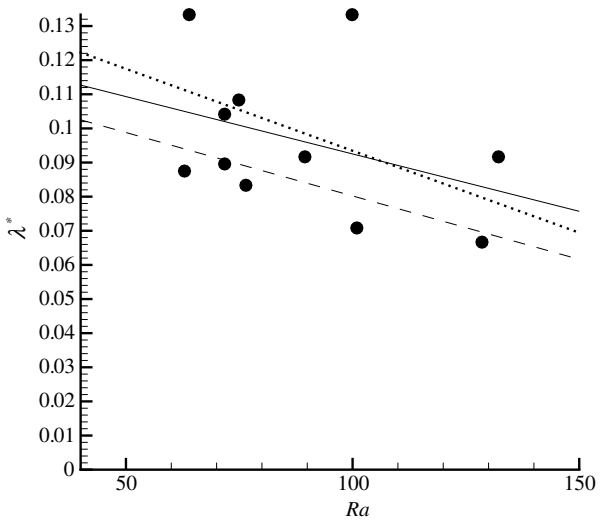

Fig. 13. Dimensional measured wavelength λ^* (○) and interpolation of the dimensional wavelength λ^* (m) versus Ra for the experimental series 11: experiment (—) and theoretical predictions for T modes with $m = 6$ (···) and pure T rolls (---).

$1 \leqslant m \leqslant 5$ lie between the curves presented in Fig. 13. It is seen that the global tendency of theoretical predictions of wavelengths for T rolls are lower than that of experiments. On the other hand, it is also seen that the predicted wavelengths for oscillatory 3D structures compare globally with experimental results. The second way we adopt for comparison is to compute wavelength for each combination of Ra and Pe with m ranging from 0 to 6. Quantitative comparisons between theory and experiment are displayed in Table 2 and indicate that the discrepancy lies between 0.5% and 14.5%. There are no fitted parameters in the comparison of theory and measurement. In view to check the predicted Ra and Pe dependence of the wavelength, we use experimental data given in Table 2:

(i) For $Ra = 72$, if we increase Pe from 7.23 to 12.25, λ^*_{exp} increases then from 8.9 to 10.4 cm.
(ii) For $Pe = 11.75$, if Ra is raised from 100.93 to 128.54, λ^*_{exp} decreases from 7.1 to 6.7 cm.

These behaviors observed in experiments confirm the predicted results summarized in Fig. 9(a).

Table 2
Comparison between the predicted and the measured dimensional wavelength λ^*_{th} and λ^*_{exp}, for different combinations of Ra and Pe

Pe	Ra	λ^*_{exp} (cm)	λ^*_{th} (cm)	Discrepancy (%)
2.56	63.95	13.3	11.46 ($m = 6$)	−13.8
7.23	72	8.9	8.8 ($m = 2$)	−1.1
12.25	72	10.4	10.43 ($m = 5$)	−0.2
8.28	74.89	10.8	10.12 ($m = 6$)	−6.3
13.86	76.40	8.4	9.61 ($m = 0$)	14.4
6.17	89.48	9.2	9.33 ($m = 6$)	1.4
11.75	100.93	7.1	8.13 ($m = 0$)	14.5
11.75	128.54	6.7	7.37 ($m = 0$)	10.
7.83	132.18	9.16	7.93 ($m = 6$)	−13.4

The temperature recordings in MC experiments allowed to measure the relative propagation speed of the rolls, U_P/U. This velocity depends both on the porosity Φ and the ratio of the heat capacity of the fluid to the heat capacity of the porous matrix, $(\rho c)_f/(\rho c)_s$. From experimental data of series 11 [8–10] found $\Phi U_P/U = 0.43$. In Section 5 we predicted that the evolution of the dimensionless phase velocity $V_\varphi = \omega_r/k_{0r}$ is almost equal to Pe. Taking into account the scaling factors for the time, the space and the filtration velocity, this yields $\Phi U_P/U = 1/[1 + (1 - \Phi)(\rho c)_s/\Phi(\rho c)_f]$. For the particular case of series 11 with $\Phi = 0.381$ and $(\rho c)_f/(\rho c)_s = 2.2$, this yields $\Phi U_P/U = 0.57$. We claim that the discrepancy between theory and experiment is due in part to the uncertainty to measure the wavelength. We expect that the remainder of the difference is explained by our idealized model which consider the bounding metal plates as isothermal. This assumption supposes that the thermal conductivity of the bounding plates is infinite, a condition that cannot be completely satisfied in actual experiments. In the context of Rayleigh–Bénard problem without shear flow, Carrière et al. [32] examined the importance of the conductivity of the horizontal boundaries on the wavelength selection. The results of this investigation indicate in particular that, as the conductivity of the fluid exceeds that of the boundary, the critical Rayleigh number and wave number decrease strongly. The influence of finite thermal conductivity of the metal plates on wavelength, frequency and phase velocity in our problem requires a further work. As a consequence of the discrepancy between predictions of the theory and experiments concerning the phase velocity, our predicted period of oscillations is always less than the measured one for actual Rayleigh number. Nevertheless, when one limits the comparison to the onset of absolute instability as shown in Fig. 14, an excellent agreement is found between the measured period of oscillations T^* and the period T^{*A} at the border between convective and absolute instability.

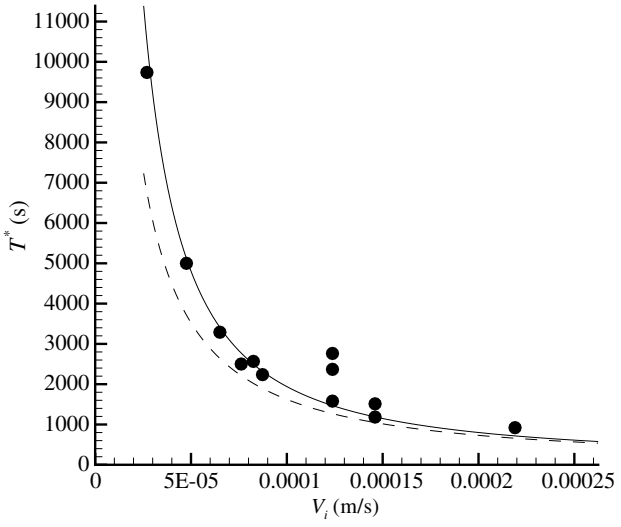

Fig. 14. Dimensional period of oscillations versus interstitial velocity V_i(m/s): experiment (○), theoretical predictions at the border between convective and absolute instability (— for $m = 6$ and ⋯ for pure T rolls).

7. Conclusion

In the present paper we investigate the stability of a fluid in porous media subject simultaneously to an horizontal through-flow and to a vertical temperature gradient. Special emphasis is given to the non-Darcian effects and to the influence of the lateral aspect ratio of the medium on the convective or absolute nature of the instability. Major results obtained in this study can be summarized as follows:

(1) As far as the perturbation is spatially extended, a temporal stability analysis indicates that the form of the instability depends on the lateral aspect ratio a. For infinite a longitudinal rolls are favored above any other structures irrespective of the values of Péclet number Pe. While with a finite a it is found that there exists a critical Péclet number Pe^* in such a way that for $Pe < Pe^*$ the oscillatory three-dimensional instability becomes unstable first and for $Pe > Pe^*$ the most unstable disturbances are longitudinal rolls. The transition that occurs at Pe^* may be smooth or abrupt depending on the aspect ratio.

(2) This picture changes drastically if, instead of considering spatially extended perturbations, localized ones are regarded as it must be the case for open flow systems. Three-dimensional spatial stability analysis is performed in this case and reveals that although moving 3D modes may experience a transition from convective to absolute instability, pure transversal rolls are the most absolutely unstable modes. We found that by increasing inertia the transition to the absolute instability is delayed substantially.
Comparison with early experiments [8–10] indicates that the theoretical transition curve from convective to absolute instability in the Rayleigh–Péclet number plane corresponds perfectly to the observed transition from moving transversal modes to stationary longitudinal rolls and vice versa. Moreover it has also been found that the measured period of oscillations of transverse modes are in a very good agreement with the theoretically predicted ones at the threshold of absolute instability. These comparisons are less satisfactory when the beads or matrix are much more conductive than the fluid. Therefore the assumption of local thermodynamic equilibrium between the two phases must be reconsidered.

(3) Far from the threshold of absolute instability we found that the wavelength, uniquely selected in laboratory experiments, agrees globally with our predictions for various Rayleigh and Péclet numbers. However, we found a discrepancy between the experimental and the theoretical propagation speed of the rolls. This suggests that an examination of the influ-

ence of finite thermal conductivity of the bounding metal plates on the moving transverse rolls is highly needed.

(4) While for infinite lateral aspect ratio longitudinal rolls remain convectively unstable whatever the values of *Pe*, the main effect of a finite aspect ratio is to create a region of absolute instability. Because numerous similarities between mixed convection in porous media and in clear fluids, we believe that this new result will encourage future research on the effects of a finite lateral aspect ratio on the convective/absolute nature of longitudinal rolls in fluid media.

References

[1] M.T. Ouazzani, J.K. Platten, A. Mojtabi, Intermittent patterns in mixed convection, Appl. Sci. Res. 51 (1993) 677–685.

[2] J.T. Lir, M.Y. Chang, T.F. Lin, Vortex flow patterns near critical state for onset of convection in air flow through a bottom heated horizontal flat duct, Int. J. Heat Mass Transfer 44 (2001) 705–719.

[3] T.C. Cheng, J.T. Lir, T.F. Lin, Stationary transverse rolls and U-rolls in limiting low Reynolds number mixed convective air flow near the convective threshold in a horizontal flat duct, Int. J. Heat Mass Transfer 45 (2002) 1211–1227.

[4] X. Nicolas, J.-M. Luijkx, J.-K. Platten, Linear stability of mixed convection flows in horizontal rectangular channels of finite transversal extension heated from below, Int. J. Heat Mass Transfer 43 (2000) 589–610.

[5] P. Carrière, P.A. Monkewitz, Convective versus absolute instability in mixed Rayleigh–Bénard–Poiseuille convection, J. Fluid Mech. 384 (1999) 243–262.

[6] X. Nicolas, Bibliographical review on the Poiseuille–Rayleigh–Bénard flows: the mixed convection flows in horizontal rectangular ducts heated from below, Int. J. Therm. Sci. 41 (2002) 961–1016.

[7] D.A. Nield, A. Bejan, Convection in Porous Media, Springer Verlag, New York, 1998.

[8] M. Combarnous, Convection naturelle et convection mixte en milieu poreux, Ph.D. thesis, Faculté des sciences de l'univ. de Paris, 1970.

[9] M. Combarnous, P. Bia, Combined free end forced convection in porous media, Soc. Petrol. Eng. J. 251 (11) (1971) 399–405.

[10] M. Combarnous, S.A. Bories, Hydrothermal convection in saturated porous media, Adv. Hydrosci. 10 (1975) 231–307.

[11] M. Prats, The effect of horizontal fluid motion on thermally induced convection currents in porous media, J. Geophys. Res. 71 (1967) 4835–4838.

[12] D.A.S. Rees, The effect of inertia on the onset of mixed convection in a porous layer heated from below, Int. Commun. Heat Mass Transfer 24 (2) (1997) 277–283.

[13] T.J. Chung, J.H. Park, C.K. Choi, D.Y. Yoon, The onset of vortex in laminar forced convection flow through a horizontal porous channel, Int. J. Heat Mass Transfer 45 (2002) 3061–3064.

[14] F. Dufour, M.C. Néel, Numerical study of instability in a horizontal porous channel with bottom heating and forced horizontal flow, Phys. Fluids 10 (9) (1998) 2198–2207.

[15] A. Delache, M.N. Ouarzazi, M. C Néel, Structuration de la convection mixte en milieu poreux confiné laté ralement et chauffé par le bas: effets d'inertie, CR Mecanique 330 (2002) 885–891.

[16] A. Delache, Etude analytique et numérique des instabilités spatio-temporelles des écoulements de convection mixte en milieu poreux: comparaison avec l'expérience, Ph.D. thesis, Université des Sciences et Technologies de Lille, 2005.

[17] D.A.S. Rees, A. Postelnicu, The onset of convection in an inclined anisotropic porous layer, Int. J. Heat Mass Transfer 44 (2001) 4127–4138.

[18] P.A. Huerre, P.A. Monkewitz, Local and global instabilities in spatially developing flows, Ann. Rev. Fluid Mech. 22 (1990) 473–537.

[19] M.N. Ouarzazi, A. Joulin, P.A. Bois, J.K. Platten, Soret effect and mixed convection in porous media, in: W. Köhler, S. Wiegand (Eds.), Thermal Non Equilibrium Phenomena in Fluid Mixtures, Lecture Notes in Physics, vol. 584, Springer, 2002, pp. 428–447.

[20] A. Joulin, M.N. Ouarzazi, Mixed convection of a binary mixture in a porous media, CR Acad. Sci. Paris, série IIb 328 (2000) 311–316.

[21] H.R. Brand, R.J. Deissler, G. Ahlers, simple model for the Bénard instability with horizontal flow near threshold, Phys. Rev. A 43 (1991) 4262–4268.

[22] H.W. Müller, M. Tveitereid, S. Trainoff, Rayleigh–Bénard problem with imposed weak through-flow: two coupled Ginzburg–Landau equations, Phys. Rev. E 48 (1993) 26–272.

[23] M. Tveitereid, H.W. Müller, Pattern selection at the onset of Rayleigh–Bénard convection in a horizontal shear flow, Phys. Rev. E 50 (1994) 1219–1226.

[24] P. Carrière, P.A. Monkewitz, D. Martinand, Envelope equations for the Rayleigh–Bénard–Poiseuille system. Part 1. Spatially homogeneous case, J. Fluid Mech. 502 (2004) 153–174.

[25] X. Nicolas, A. Mojtabi, J.K. Platten, Two-dimensional numerical analysis of the Poiseuille–Bénard flow in a rectangular channel heated from below, Phys. Fluids 9 (2) (1997) 337–348.

[26] E. Schröder, K. Bühler, Three-dimensional convection in rectangular domains with horizontal through-flow, Int. J. Heat Mass Transfer 38 (1995) 1249–1259.

[27] J.M. Luijkx, J.K. Platten, J.C. Legros, On the existence of thermoconvective rolls, transverse to a superimposed mean Poiseuille flow, Int. J. Heat Mass Transfer 24 (7) (1981) 1287–1291.

[28] M. Combarnous, S. Bories, Modélisation de la convection naturelle au sein d'une couche poreuse horizontale à l'aide d'un coefficient de transfert solide-fluide, Int. J. Heat Mass Transfer 17 (1974) 505–515.

[29] Nurzahan Banu, D.A.S. Rees, Onset of Darcy–Bénard convection using a thermal non-equilibrium model, Int. J. Heat Mass Transfer 45 (2002) 2221–2228.

[30] J.M. Chomaz, Fully nonlinear dynamics of parallel wakes, J. Fluid Mech. 495 (2003) 57–75.

[31] H.W. Müller, M. Lücke, M. Kamps, Transversal convection patterns in horizontal shear flow, Phys. Rev. A 45 (6) (1992) 3714–3726.

[32] P. Carrière, A. Bottaro, P. Metzener, Wavelength selection in Rayleigh–Bénard convection between horizontal boundaries of finite conductivity, Eur. J. Mech. B/Fluids 16 (4) (1997) 483–508.